

# Journal of Materials Chemistry A

Accepted Manuscript



This is an *Accepted Manuscript*, which has been through the Royal Society of Chemistry peer review process and has been accepted for publication.

*Accepted Manuscripts* are published online shortly after acceptance, before technical editing, formatting and proof reading. Using this free service, authors can make their results available to the community, in citable form, before we publish the edited article. We will replace this *Accepted Manuscript* with the edited and formatted *Advance Article* as soon as it is available.

You can find more information about *Accepted Manuscripts* in the [Information for Authors](#).

Please note that technical editing may introduce minor changes to the text and/or graphics, which may alter content. The journal's standard [Terms & Conditions](#) and the [Ethical guidelines](#) still apply. In no event shall the Royal Society of Chemistry be held responsible for any errors or omissions in this *Accepted Manuscript* or any consequences arising from the use of any information it contains.

## High voltage in hole conductor free organo metal halide perovskite solar cells

Alex Dymshits, Amit Rotem, Lioz Etgar\*

The Hebrew University of Jerusalem, Institute of Chemistry, Casali Center for Applied Chemistry, Jerusalem 91904, Israel

\* [lnoz.etgar@mail.huji.ac.il](mailto:lnoz.etgar@mail.huji.ac.il)

### Abstract

Organo metal halide perovskite has attracted much attention recently due to distinctive properties that make it especially useful in photovoltaic solar cells. In this work we demonstrate high open circuit voltage of 1.35V using  $\text{Al}_2\text{O}_3/\text{CH}_3\text{NH}_3\text{PbBr}_3$  perovskite solar cells without a hole conductor. The contact potential difference under light measured by surface photovoltage spectroscopy for  $\text{CH}_3\text{NH}_3\text{PbBr}_3$  was more than twice than that for  $\text{CH}_3\text{NH}_3\text{PbI}_3$ , which results with smaller surface potential for the  $\text{Al}_2\text{O}_3/\text{CH}_3\text{NH}_3\text{PbBr}_3$  cells. Incident modulated photovoltage spectroscopy shows a longer recombination lifetime for the  $\text{Al}_2\text{O}_3/\text{CH}_3\text{NH}_3\text{PbBr}_3$  cells than for the  $\text{TiO}_2/\text{CH}_3\text{NH}_3\text{PbI}_3$  cells or for the  $\text{TiO}_2/\text{CH}_3\text{NH}_3\text{PbBr}_3$  cells, further supporting the high open circuit voltage. The possibility to gain high open circuit voltage even without a hole transport material in perovskite solar cells shows that the perovskite/metal oxide interface has a major effect on the open circuit voltage in perovskite based solar cells.

### Introduction

Alternative energy is an important research area and will remain so for the foreseeable future, and photovoltaics (PV) are a key technology for a sustainable energy supply. A PV device is based on the photoelectric effect, requiring photo-generation of charge carriers (electrons and holes) in a light-absorbing material and their separation to conductive contacts that transmit electricity. A breakthrough has occurred in recent years as a promising new material, organo metal halide perovskite, is being used in the solar cells, achieving approximately 18% efficiency.<sup>1</sup> Interestingly, the perovskite isn't restricted to specific solar cell architecture and can be used with different metal oxides, where injection of electrons is possible and where the metal oxide functions as a scaffold.<sup>2,3,4</sup> Moreover, a long-range electron-hole diffusion length was found in organometal perovskite absorber, which might explain the high efficiency achieved for perovskite based solar cells<sup>5,6</sup>. Other reports demonstrate that the use of the perovskite

both as a light harvester and as a hole conductor eliminates the use of hole transport material (HTM), achieving more than 10% efficiency.<sup>7,8,9</sup>

One of the attractive properties of organo metal halide perovskite is its ability to gain high open circuit voltage ( $V_{oc}$ ) with a high ratio of  $qV_{oc}/E_g$ .  $V_{oc}$  of 1.15 V was achieved with a cell that used  $CH_3NH_3PbBr_3$  as sensitizer/absorber, with poly[N-9-heptadecanyl-2,7-carbazole-alt-3,6-bis-(thiophen-5-yl)-2,5-dioctyl-2,5-dihydropyrrolo[3,4-pyrrole-1,4-dione] (PCBTDPP) as hole transport material.<sup>10</sup> An even higher open circuit voltage of 1.3 V resulted when using N,N'-dialkylperylene diimide (PDI) as hole transport material with  $CH_3NH_3PbBr_3$  as the sensitizer/absorber<sup>11</sup>. Recently 1.5V was reported when using  $CH_3NH_3PbBr_{3-x}Cl_x$  with 4,4'-bis(N-carbazolyl)-1,1'-biphenyl (CBP) as hole conductor<sup>12</sup>. Both high efficiency (6.7%) and high voltage (1.4V) was demonstrated with hole transport material based on tri-arylamine (TAA) polymer derivatives containing fluorene and indenofluorene.<sup>13</sup> All the reports mentioned relating to high voltage based on perovskite use hole transport material to tune and to gain high  $V_{oc}$ . However, is it possible to get high  $V_{oc}$  without hole transport material? Based on recent reports,<sup>12,13</sup> the voltage in the perovskite solar cells isn't determined simply by the difference between the  $TiO_2$  fermi level and the fermi level of the HTM. Therefore, it could be that high  $V_{oc}$  can be achieved in perovskite based solar cells even without HTM.

In this work, we demonstrate a high  $V_{oc}$  of 1.35V for perovskite solar cells without a hole conductor. Several combinations of metal oxides/perovskites are studied. Surface photovoltage and incident modulated photovoltage spectroscopy are used to elucidate the reason for the high voltage achieved for these hole conductor free cells.

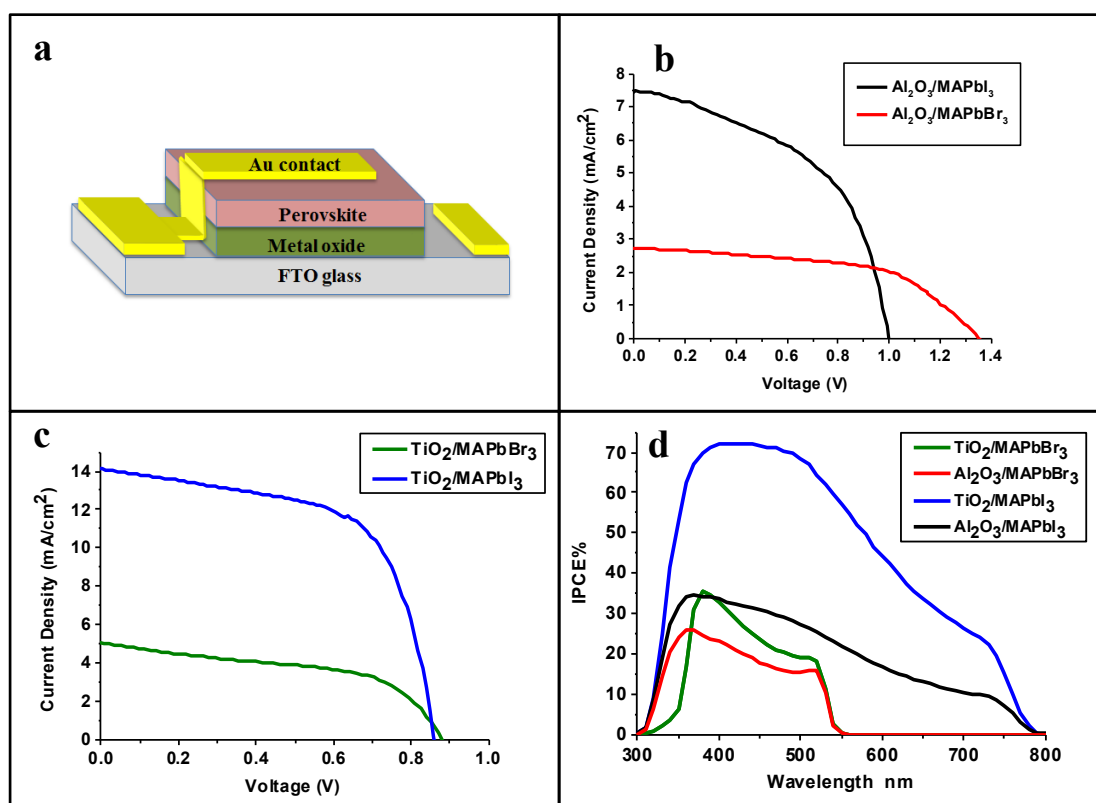
## Results and discussion

Figure 1a shows a schematic illustration of the high voltage hole conductor free perovskite solar cell. The bottom layer is composed of conductive glass with a  $TiO_2$  compact layer; then a thin film of nanocrystalline metal oxide  $TiO_2$  or  $Al_2O_3$  was deposited. The  $CH_3NH_3PbI_3$  or  $CH_3NH_3PbBr_3$  ( $CH_3NH_3=MA$ ) perovskites were deposited by the two-step deposition as described earlier.<sup>14,15</sup> Finally, a metal contact was evaporated directly on top of the perovskite. As our previous work shows,<sup>9</sup> the perovskite functions both as light harvester and hole conductor, eliminating the use of hole transport material.

Figures 1b-d and table 1 present the photovoltaic parameters and the incident photon to current efficiency (IPCE) achieved for the high voltage cells. Four different combinations were studied—nanocrystalline  $\text{TiO}_2$  with  $\text{MAPbI}_3$  and  $\text{MAPbBr}_3$ , and nanocrystalline  $\text{Al}_2\text{O}_3$  with both perovskites. The open circuit voltage ( $V_{oc}$ ) for the cells with the  $\text{MAPbBr}_3$  perovskite deliver higher voltages compared with the cells with the  $\text{MAPbI}_3$  perovskite related to the same metal oxide. Moreover, the cells with  $\text{Al}_2\text{O}_3$  achieve higher  $V_{oc}$  compared to the  $\text{TiO}_2$  based cells. The highest  $V_{oc}$  observed for the  $\text{Al}_2\text{O}_3/\text{MAPbBr}_3$  configuration achieved 1.35V without a hole conductor. This is the highest reported open circuit voltage for perovskite cells without a hole conductor and is comparable to cells using hole transport material. It is important to note that the average  $V_{oc}$  (including more than 11 cells) for the  $\text{Al}_2\text{O}_3/\text{MAPbBr}_3$  configuration is  $1.24 \pm 0.08$  V with 4 cells having  $V_{oc}$  of more than 1.3V and 4 cells with  $V_{oc}$  higher than 1.21V. High power conversion efficiency (PCE) with high voltage was observed for the  $\text{Al}_2\text{O}_3/\text{MAPbI}_3$  configuration achieving PCE of 4.1% with  $V_{oc}$  of 1V. The IPCE spectra show typical behavior with coverage until 550 nm wavelength for the  $\text{MAPbBr}_3$  and until 780nm wavelength for the  $\text{MAPbI}_3$ .

Table 1: Photovoltaic parameters of the hole conductor free solar cells studied.

|   | $\eta(\%)$ | Fill Factor | $J_{sc}$ ( $\text{mA}/\text{cm}^2$ ) | $V_{oc}$ (V) |
|---|------------|-------------|--------------------------------------|--------------|
| $\text{TiO}_2/\text{MAPbI}_3$           | 7.5        | 0.61        | 14.1                                 | 0.86         |
| $\text{TiO}_2/\text{MAPbBr}_3$          | 1.88       | 0.49        | 4.37                                 | 0.87         |
| $\text{Al}_2\text{O}_3/\text{MAPbI}_3$  | 4.13       | 0.5         | 7.46                                 | 1.0          |
| $\text{Al}_2\text{O}_3/\text{MAPbBr}_3$ | 2.02       | 0.55        | 2.7                                  | 1.35         |



**Figure 1:** (a) The solar cell structure. (B) JV curves of the cells made with Al<sub>2</sub>O<sub>3</sub> as a scaffold. (c) Cells made with TiO<sub>2</sub>. (d) The corresponding IPCE curves.

Figures 2a-b show the energy level diagram for the four different cases described in this paper. Figure 2a presents the MAPbBr<sub>3</sub> and MAPbI<sub>3</sub> deposited on Al<sub>2</sub>O<sub>3</sub> which function as a scaffold; electron injection from the perovskite to the Al<sub>2</sub>O<sub>3</sub> isn't possible in this configuration. Figure 2b presents the MAPbBr<sub>3</sub> and MAPbI<sub>3</sub> with TiO<sub>2</sub>, where electron injection from the perovskite to the TiO<sub>2</sub> is favorable. Surface photovoltage (SPV) was used to measure the work function of the Al<sub>2</sub>O<sub>3</sub>, TiO<sub>2</sub>, MAPbI<sub>3</sub> and MAPbBr<sub>3</sub>; the calculated work functions are shown as red lines in figure 2. The work function positions (which are the Fermi level positions) correspond well to the p-type behavior of the MAPbBr<sub>3</sub> and MAPbI<sub>3</sub> perovskites, and the n-type behavior of the TiO<sub>2</sub> as discussed below. Figures 2c and 2d show the corresponding high resolution scanning electron microscopy (HR-SEM) cross sections of the Al<sub>2</sub>O<sub>3</sub>/MAPbI<sub>3</sub> and Al<sub>2</sub>O<sub>3</sub>/MAPbBr<sub>3</sub> HTM free cells, the perovskite over layer can be observed clearly. The HR-SEM cross sections of the TiO<sub>2</sub> based cells are shown in the supporting information. (Figure 2S)

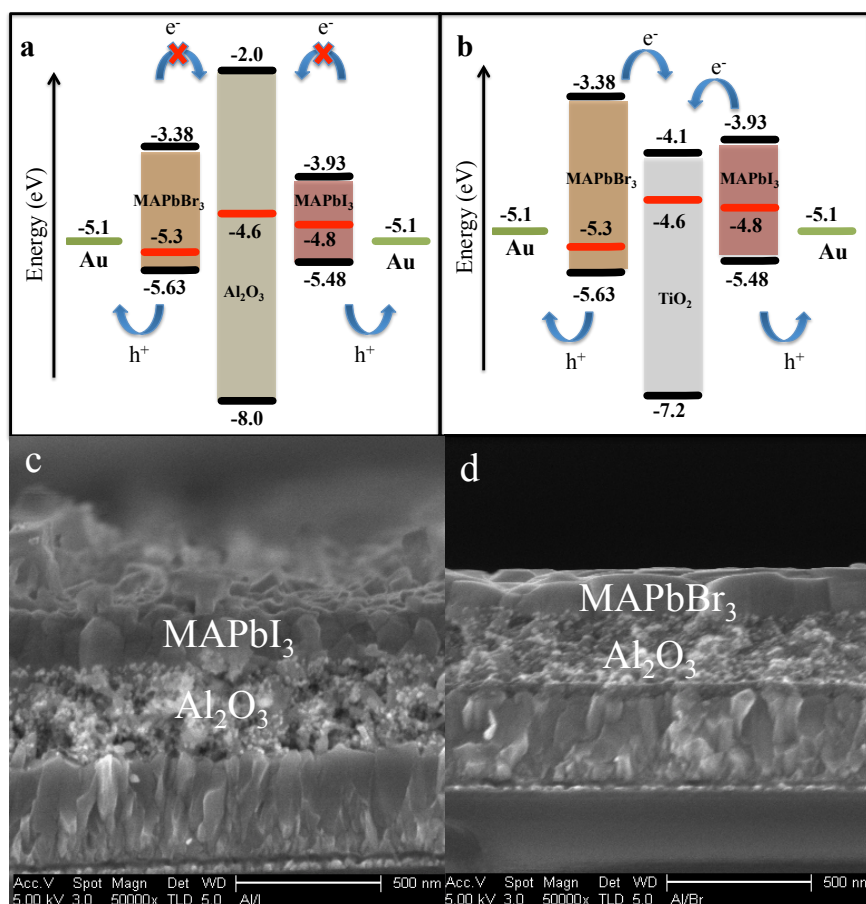


**Figure 2:** (a,b) Energy level diagram of the different cells. Fermi levels measured under dark are presented in red in the figure. The position of the conduction and valence bands are according to ref. 13. (c) HR-SEM cross section of  $\text{Al}_2\text{O}_3/\text{MAPbI}_3$  HTM free cell. (d) HR-SEM cross section of  $\text{Al}_2\text{O}_3/\text{MAPbBr}_3$  HTM free cell.

Surface photovoltage (SPV) spectroscopy and incident modulated photovoltage spectroscopy (IMVS) were performed to gain more information about the reason for the high open circuit voltage when no HTM is used. Previous studies already demonstrate high  $V_{oc}$  in perovskite cells contain HTM. It was suggested that the  $V_{oc}$  is not merely the difference between the hole Fermi level of the hole conductor and the electron Fermi level of the nanocrystalline  $\text{TiO}_2$ .<sup>13,16</sup> Moreover, it was reported that charges could be accumulated in the perovskite due to its high capacitance, which allows the control of the quasi Fermi level during illumination.<sup>17</sup>

The SPV technique is based on Kelvin probe, which measures the difference in work functions (also known as the contact potential difference (CPD)) between a metallic reference probe and semiconductor surface. The metallic probe is vibrates which formed a capacitor arrangement between the reference electrode and the semiconductor (the distance between them is few millimeter). This results in an AC current in the

external circuit. If there is no charge on the capacitor the AC current is zero. In this case, the CPD must be zero. The AC current is nullified when a DC bias is applied. Thus, the applied DC bias is equal and opposite to the CPD. (please see figure 3S in the supporting information for schematic explanation)

The SPV spectra of the MAPbI<sub>3</sub> and MAPbBr<sub>3</sub> are shown in figure 3a, with the estimated band gaps shown as vertical lines. Several observations result from the SPV spectra (figure 3a). First, the spectra provide information about the band gaps of the materials, equivalent to the information observed from the absorption spectra (figure S1 in the Supporting Information). Second, the sign of the SPV signal indicates the samples type. The surface work function is changed on illumination. It decreases for the n-type semiconductor—TiO<sub>2</sub> in this case—and increases for the p-type semiconductor, the MAPbI<sub>3</sub> and MAPbBr<sub>3</sub> in this case. A third important observation is related to the unique property of the SPV method, its immunity to reflection or scattering losses only photons that are absorbed in the sample contribute to the SPV signal. In this case the signal onset starts at photon energies very close to the band gap of the perovskite samples (the MAPbI<sub>3</sub> and the MAPbBr<sub>3</sub>), and as a result, it can be concluded that the perovskite samples have fewer sub-bandgap states. The relation  $qV_{oc}/E_g$  is the ratio of the maximum voltage developed by the solar cell ( $V_{oc}$ ) to the voltage related to the band-gap of the absorber ( $E_g/q$ ). For the Al<sub>2</sub>O<sub>3</sub>/MAPbBr<sub>3</sub> cell the  $qV_{oc}/E_g$  is 0.61, compared to recent reports of high voltage perovskite cells with HTM shown as  $qV_{oc}/E_g$  of 0.55 and 0.73.<sup>11,12</sup> Our results demonstrate comparable values with respect to the values obtained with HTM.

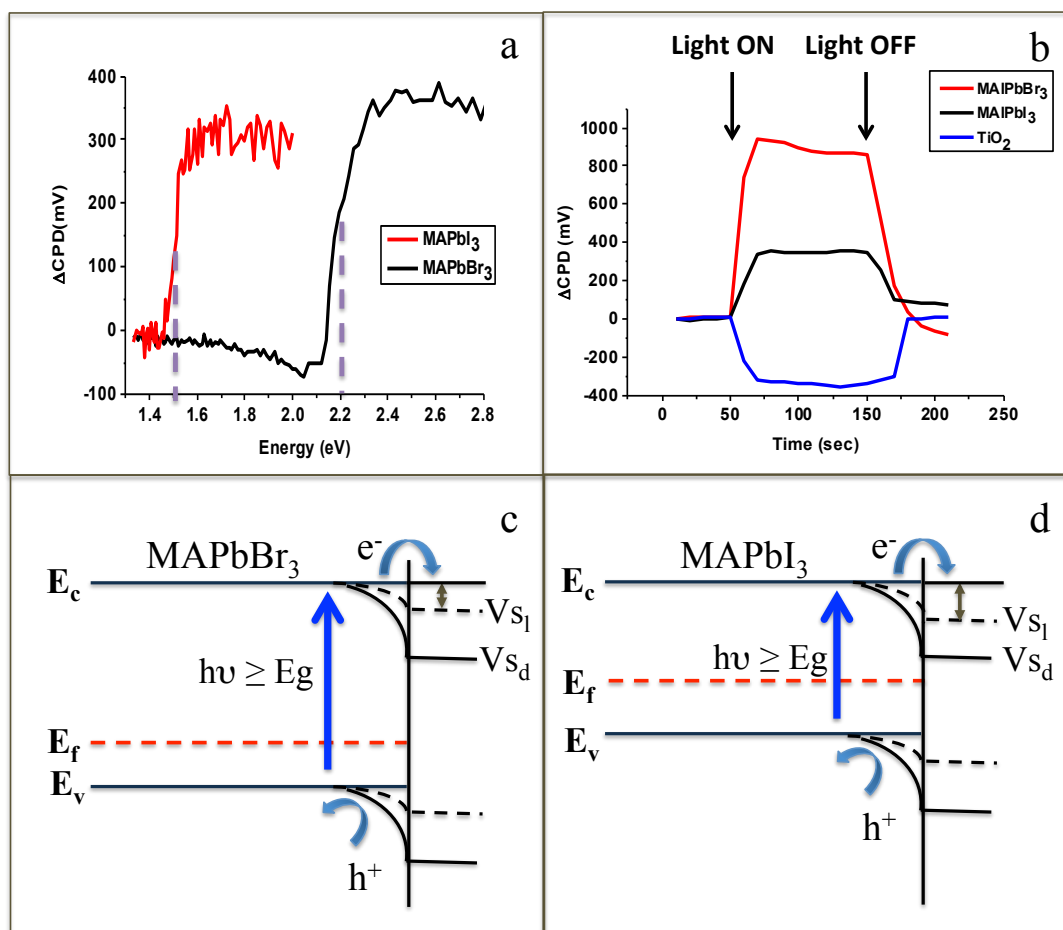


**Figure 3:**(a) SPV spectra of the MAPbI<sub>3</sub> and MAPbBr<sub>3</sub> films with estimated band gaps, 1.55eV and 2.2eV, respectively. (b) Contact potential difference (CPD) change with white light switched on and off for the samples studied. (c) The effect of band-to-band transitions on the surface photovoltage responses of MAPbBr<sub>3</sub> and (d) MAPbI<sub>3</sub>. V<sub>Sd</sub>- surface potential in the dark, V<sub>S1</sub>- surface potential in light.

The  $qV_{oc}/E_g$  relation in the case of the cells based Al<sub>2</sub>O<sub>3</sub> are 0.64 and 0.61 for the MAPbI<sub>3</sub> and MAPbBr<sub>3</sub> respectively and for the TiO<sub>2</sub> based cells 0.55 and 0.37 for MAPbI<sub>3</sub> and MAPbBr<sub>3</sub> respectively. Based on these values it can be observed that the Al<sub>2</sub>O<sub>3</sub>/MAPbBr<sub>3</sub> based cells have slightly more thermal losses than the Al<sub>2</sub>O<sub>3</sub>/MAPbI<sub>3</sub> cells, moreover high thermal losses were observed in the TiO<sub>2</sub> based cell compared to the Al<sub>2</sub>O<sub>3</sub> based cells.

Figure 3b presents the contact potential difference (CPD) change when a light is switched on and off. The SPV onset  $t_{on}$  and  $t_{off}$  are below the resolution limit of the measurements system. Our observations from these measurements are related to the change in the CPD—for the TiO<sub>2</sub> sample, a negative change in the CPD was observed, while for the perovskites samples, a positive change in the CPD was observed,



corresponding to their electronic behavior. The  $\Delta\text{CPD}$  for the  $\text{MAPbI}_3$  is 350 mV and the  $\Delta\text{CPD}$  for the  $\text{MAPbBr}_3$  is 850 mV.

The  $V_s$  presented in figure 3c and 3d is the surface potential barrier (where  $V_{s_d}$  is the surface potential in the dark and  $V_{s_l}$  is the surface potential in light), which measured in the SPV experiment. The difference between the surface potential in the light ( $V_{s_l}$ ) and in the dark ( $V_{s_d}$ ) is defined as the SPV signal. In super band gap illumination photons with energy equal or larger than the band gap hit the material and generate electron-hole pairs, which collected by the surface barrier, consequently the surface potential is reduced. The trap to band transition is neglected in super band gap illumination while the band-to-band absorption is the dominant one.

Figure 3c and 3d shows the effect of band-to-band transition on the SPV response of  $\text{MAPbBr}_3$  and  $\text{MAPbI}_3$  respectively. Under illumination there is redistribution of surface charges, which decrease the bend bending, and as a result the SPV response is generated. According to the  $\Delta\text{CPD}$  shown in figure 3b the surface potential for the  $\text{MAPbBr}_3$  is smaller than the surface potential for the  $\text{MAPbI}_3$  as indicated by the bi directional arrow in figures 3c and 3d respectively. (This is also seen by the bend bending reduction, since the difference between  $V_{s_l}$  to  $V_{s_d}$  is larger in the case of  $\text{MAPbBr}_3$ ) The reduction of the surface potential observed from the SPV measurements for the HTM free  $\text{MAPbBr}_3$  cells, could be a possible contribution to the higher  $V_{oc}$  achieved for these cells.

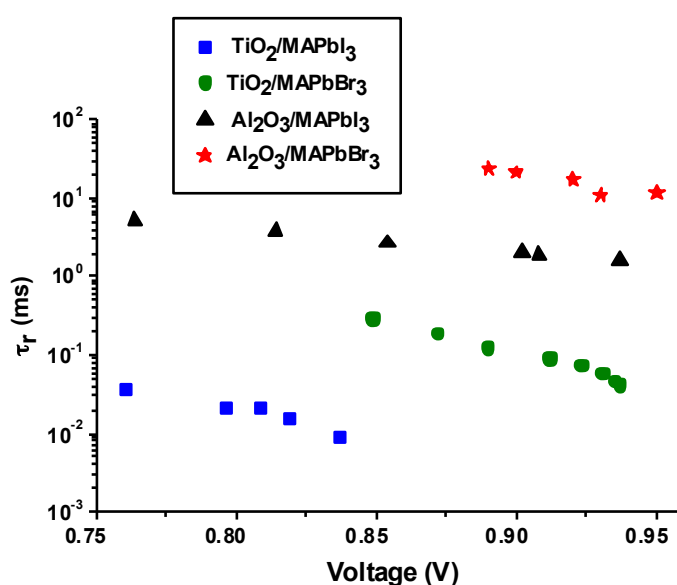


**Figure 4:** Recombination lifetime ( $\tau_r$ ) as a function of the open circuit voltage for the cells studied, measured by IMVS.

Further contribution for the difference in the open circuit voltage is presented in figure 4. The recombination lifetime ( $\tau_r$ ) as a function of the voltage were calculated by IMVS.<sup>18,19,20</sup> All cells showed the same dependence of electron recombination lifetime (which are the minority carrier) by the voltage, the decrease of the recombination lifetime with increasing the voltage. This behavior can be attributed to the increased recombination with the higher electron density.<sup>18</sup> However the  $\tau_r$  values are different for the various cells; in particular, the lower  $\tau_r$  values were observed for the TiO<sub>2</sub>/MAPbI<sub>3</sub> cell, which also had the lower  $V_{oc}$ . The highest  $\tau_r$  values were observed for the Al<sub>2</sub>O<sub>3</sub>/MAPbBr<sub>3</sub> cell, which result with less recombination (since the lifetime for recombination is longer) corresponding with the highest voltage observed. Longer recombination lifetime ( $\tau_r$ ) will decrease the recombination, which could result in higher  $V_{oc}$ <sup>21,22</sup>. In addition, longer recombination lifetimes were observed for the cells with the Al<sub>2</sub>O<sub>3</sub> as a scaffold, compared to cells with mesoporous TiO<sub>2</sub>, which could contribute to the higher voltages observed in the case of Al<sub>2</sub>O<sub>3</sub> based cells. This is consistent with the  $qV_{oc}/E_g$  relation as discussed above, which more thermal losses were observed for cells based TiO<sub>2</sub> as the metal oxide compare to cells based Al<sub>2</sub>O<sub>3</sub>.

## Conclusions

In this work, high voltage of 1.35V was observed for hole conductor free perovskite solar cells. SPV and IMVS techniques were used to elucidate the origin of the high voltage observed. The Fermi level position and the SPV spectra of the MAPbI<sub>3</sub> and MAPbBr<sub>3</sub> reveal the p-type behavior of these perovskites. The CPD change when light was switched on and off was higher by a factor of 2.5 for the MAPbBr<sub>3</sub> cells compared to the MAPbI<sub>3</sub> cells. The change in the CPD during illumination results with smaller surface potential for the Al<sub>2</sub>O<sub>3</sub>/MAPbBr<sub>3</sub> cells, which could contribute to the higher open circuit voltage achieved in the MAPbBr<sub>3</sub> cells. Further support was observed by longer recombination lifetime for the Al<sub>2</sub>O<sub>3</sub> based cells, compared to cells with mesoporous TiO<sub>2</sub>. The high open circuit voltage observed in cells without a hole conductor indicates that the origin of the open circuit voltage is affected by the perovskite and the perovskite/metal oxide interface.

## Experimental

### Material synthesis

The Al<sub>2</sub>O<sub>3</sub> nanoparticles (<50 nm particle size, Sigma-Aldrich) were dissolved in isopropanol at a concentration of 20 wt%. The Al<sub>2</sub>O<sub>3</sub> nanoparticles were deposited by spin coating at 2000 r.p.m. for 10 s and annealed at 500 °C for 30 min. For the TiO<sub>2</sub> films DYESOL DSL 90-T paste was used. The TiO<sub>2</sub> paste was diluted in ethanol in a ratio of 1:4 by weight. The deposition and the annealing conditions were the same as for the Al<sub>2</sub>O<sub>3</sub>.

CH<sub>3</sub>NH<sub>3</sub>I and CH<sub>3</sub>NH<sub>3</sub>Br were synthesized as described previously<sup>23,24</sup> by reacting 30 mL of methylamine (40% in methanol, TCI) and 32.3 mL of hydroiodic acid (57 wt% in water, Aldrich) or 23.32 mL of hydrobromic acid (48 wt % in water, Aldrich) in a 250 mL round bottom flask at 0 °C for 2 h with stirring. The precipitate was recovered by putting the solution on a rotavap and carefully removing the solvents at 50 °C. The product of methylammonium iodide (CH<sub>3</sub>NH<sub>3</sub>I) or methylammonium bromide (CH<sub>3</sub>NH<sub>3</sub>Br) was washed with ethanol by stirring the mixture for 30 min. Then the mixture was filtered and washed three times with diethylether. After filtration, the solid was collected and dried at 70 °C in a vacuum oven for 24 h.

### Device fabrication

The substrate of the device was a SNO<sub>2</sub>:F (FTO) conducting glass (15Ω·cm<sup>-1</sup>, Pilkington). A blocking layer was deposited on the FTO glass using a solution of

titanium diisopropoxidebis(acetylacetonate) (TiDIP, 75% in isopropanol, Aldrich) in ethanol. The TiDIP solution was spin coated and then annealed at 450°C for 35 min. The TiO<sub>2</sub> solution or the Al<sub>2</sub>O<sub>3</sub> solution was spin coated and annealed at 500°C for 30 min, subsequent to TiCl<sub>4</sub> treatment for 30 min at 70°C and annealing at 500°C for 30 min.

The synthesis of the CH<sub>3</sub>NH<sub>3</sub>PbI<sub>3</sub> and the CH<sub>3</sub>NH<sub>3</sub>PbBr<sub>3</sub> on the TiO<sub>2</sub> surface was carried out by a two-step deposition technique.

First, PbI<sub>2</sub> or PbBr<sub>2</sub> was dissolved in DMF and dropped onto the TiO<sub>2</sub> or the Al<sub>2</sub>O<sub>3</sub> film and spin coated, followed by annealing at 70°C for 30 min. In the second step, the cell was dipped into methylammonium solution. Following the dipping step, the samples were annealed at 70°C for another 30 min. Finally, the back contact was deposited by evaporating 50 nm of gold under pressure of 5\*10<sup>-6</sup>Torr. The active area was 0.09 cm<sup>2</sup>.

### Photovoltaic characterization

Photovoltaic measurements were made on a New Port system, composed of an Oriel I-V test station using an Oriel Sol3A simulator. The solar simulator is class AAA for spectral performance, uniformity of irradiance, and temporal stability. The solar simulator is equipped with a 450 W xenon lamp. The output power is adjusted to match AM1.5 global sunlight (100 mWcm<sup>-2</sup>). The spectral match classifications are IEC60904-9 2007, JIC C 8912, and ASTM E927-05. I-V curves were obtained by applying an external bias to the cell and measuring the generated photocurrent with a Keithley model 2400 digital source meter. The voltage step and delay time of photocurrent were 10 mV and 40 ms, respectively. Oriel IQE-200 was used to determine the monochromatic incident photon-to-electric current conversion efficiency. Under full computer control, light from a 150 W xenon arc lamp was focused through a monochromator in the 300 nm–1800 nm wavelength range onto the photovoltaic cell under test. The monochromator was incremented through the visible spectrum to generate the IPCE ( $\lambda$ ) as defined by  $IPCE(\lambda) = 12,400 (J_{sc}/\lambda \phi)$ , where  $\lambda$  is the wavelength,  $J_{sc}$  is the short-circuit photocurrent density (mA cm<sup>-2</sup>), and  $\phi$  is the incident radiative flux (mWcm<sup>-2</sup>). Photovoltaic performance was measured by using a metal mask with an aperture area of 0.09 cm<sup>2</sup>.

### Surface photovoltage

Surface photovoltage spectroscopy (SPS) and work function were performed using SKP5050-SPS040 system. The contact potential difference (CPD) between the sample and vibrating tip was measured by Kelvin probe technique. Samples were measured in a

Faraday cage under air environment. For SPS measurements, the samples were illuminated with a 150W quartz tungsten halogen lamp. The wavelength resolution was 2 nm. Before measurement, samples were stabilized with a tip for about an hour. The scan direction was from long to short wavelength. The WF was calculated according to:  $WF_{\text{sample}} = WF_{\text{tip}} - CPD_{(\text{tip-sample})}$ . The WF function of the tip was calibrated above gold stage.

### **Intensity modulated photovoltage spectroscopy**

The photocarrier recombination times at open circuit were measured by intensity modulated photovoltage spectroscopy (IMVS). The IMVS measurements were performed with the Autolab FRA32M LED driver using a cool white light source, illuminating from the substrate side. The photovoltaic cells were illuminated with a bias light intensity with a 10% sinusoidal wave modulation, with frequencies ranging from 1 Hz to 20 kHz.

**High Resolution Scanning Electron Microscopy (HR-SEM):** the images were obtained using Sirion HR-SEM of FEI (Field Emission Instruments), The Netherlands. The measurement conditions were 5 kV at various magnifications, as seen on the data bar of the images.

### **Acknowledgements**

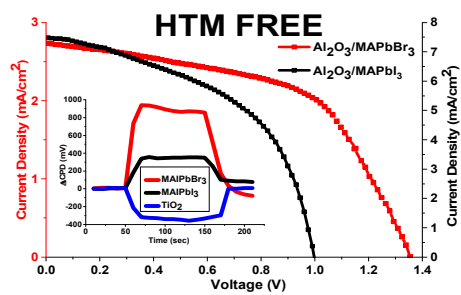
We would like to thank the Israel Alternative Energy Foundation (I-SAEF) that financed this research, the Ministry of Industry Trade and Labor Office of the Chief Scientist Kamin project No.50303, and the Tashtiot project of the Office of the Chief Scientist.

## References

- <sup>1</sup>[http://www.nrel.gov/ncpv/images/efficiency\\_chart.jpg](http://www.nrel.gov/ncpv/images/efficiency_chart.jpg)
- <sup>2</sup>Lee, M.; Teuscher, M. J.; Miyasaka, T.; Murakami, T. N.; Snaith, H. J. Efficient Hybrid Solar Cells Based on Meso-Superstructured Organometal Halide Perovskites. *Science* 2012, 338, 643-644.
- <sup>3</sup>James M. Ball, Michael M. Lee, Andrew Hey and Henry J. Snaith, Low-temperature processed meso-superstructured thin-film perovskite solar cells, *Energy & Environmental Science*, 2013, DOI: 10.1039/c3ee40810h.
- <sup>4</sup>Jin Hyuck Heo, Sang Hyuk Im, Jun Hong Noh, Tarak N. Mandal, Choong-Sun Lim, Jeong Ah Chang, Yong Hui Lee, Hi-jung Kim, Arpita Sarkar, Md. K. Nazeeruddin, Michael Grätzel & Sang Il Seok, Efficient inorganic-organic hybrid heterojunction solar cells containing perovskite compound and polymeric hole conductors, *Nature Photonics* 2013, 7, 486-491.
- <sup>5</sup>Samuel D. Stranks, Giles E. Eperon, Giulia Grancini, Christopher Menelaou, Marcelo J. P. Alcocer, Tomas Leijtens, Laura M. Herz, Annamaria Petrozza, Henry J. Snaith, Electron-Hole Diffusion Lengths Exceeding 1 Micrometer in an Organometal Trihalide Perovskite Absorber, *Science* 2013, 342, 341.
- <sup>6</sup>Guichuan Xing, Nripan Mathews, Shuangyong Sun, Swee Sien Lim, Yeng Ming Lam, Michael Grätzel, Subodh Mhaisalkar, Tze Chien Sum, Long-Range Balanced Electron- and Hole-Transport Lengths in Organic-Inorganic  $\text{CH}_3\text{NH}_3\text{PbI}_3$ , *Science* 2013, 342, 344.
- <sup>7</sup>Etgar, L.; Gao, P.; Xue, Z.; Peng, Q.; Chandiran, A. K.; Liu, B.; Nazeeruddin, Md. K.; Grätzel, M. Mesoscopic  $\text{CH}_3\text{NH}_3\text{PbI}_3/\text{TiO}_2$  Heterojunction Solar Cells. *J. Am. Chem. Soc.* 2012, 134, 17396-17399.
- <sup>8</sup>Walleed Abu Laben, Lioz Etgar. Depleted hole conductor-free lead halide iodide heterojunction solar cell, *Energy Environ. Sci.*, 2013, DOI:10.1039/C3EE42282H.
- <sup>9</sup> Sigalit Aharon, Shany Gamliel, Bat El Cohen and Lioz Etgar, *Phys. Chem. Chem. Phys.*, 2014, 16, 10512.
- <sup>10</sup> Bing Cai, Yedi Xing, Zhou Yang, Wen-Hua Zhang and Jieshan Qiu, High performance hybrid solar cells sensitized by organolead halide perovskites, *Energy Environ. Sci.*, 2013, 6, 1480.
- <sup>11</sup>Eran Edri, Saar Kirmayer, David Cahen, and Gary Hodes, High Open-Circuit Voltage Solar Cells Based on Organic-Inorganic Lead Bromide Perovskite, *J. Phys. Chem. Lett.* 2013, 4, 897-902.
- <sup>12</sup>Eran Edri, Saar Kirmayer, Michael Kulbak, Gary Hodes, and David Cahen, Chloride Inclusion and Hole Transport Material Doping to Improve Methyl Ammonium Lead Bromide Perovskite-Based High Open-Circuit Voltage Solar Cells, *J. Phys. Chem. Lett.*, 2014, 5, 429-433.
- <sup>13</sup>Seungchan Ryu, Jun Hong Noh, Nam Joong Jeon, Young Chan Kim, Woon Seok Yang, Jang won Seo and Sang Il Seok, Voltage output of efficient perovskite solar cells with high open-circuit voltage and fill factor, *Energy & environmental science*, 2014, DOI: 10.1039/c4ee00762j.
- <sup>14</sup>Bat-El Cohen, Shany Gamliel, and Lioz Etgar, Parameters influencing the deposition of methylammonium lead halide iodide in hole conductor free perovskite-based solar cells, *APL Materials*, 2014, 2, 081502.
- <sup>15</sup>J. Burschka, N. Pellet, S.-J. Moon, R. Humphry-Baker, P. Gao, M. K. Nazeeruddin, and M. Graetzel, *Nature*, 2013, 499, 316.

- <sup>16</sup>Yi-Fang Chiang, Jun-Yuan Jeng, Mu-Huan Lee, Shin-Rung Peng, Peter Chen, Tzung-Fang Guo, Ten-Chin Wen, Yao-Jane Hsu and Ching-Ming Hsu, High voltage and efficient bilayer heterojunction solar cells based on an organic–inorganic hybrid perovskite absorber with a low-cost flexible substrate, *Phys.Chem.Chem.Phys.*, **2014**, 16, 6033.
- <sup>17</sup>Hui-Seon Kim, Ivan Mora-Sero, Victoria Gonzalez-Pedro, Francisco Fabregat-Santiago, Emilio J. Juarez-Perez, Nam-Gyu Park & Juan Bisquert, Mechanism of carrier accumulation in perovskite thin-absorber solar cells, *Nature communications*, **2013**, DOI: 10.1038/ncomms3242.
- <sup>18</sup>Zhu, K.; Jang, S.-R.; Frank, A. J. Impact of High Charge- Collection Efficiencies and Dark Energy-Loss Processes on Transport, Recombination, and Photovoltaic Properties of Dye-Sensitized Solar Cells. *J. Phys. Chem. Lett.* **2011**, 2, 1070–1076.
- <sup>19</sup>Zhao, Y.; Zhu, K. Charge Transport and Recombination in Perovskite (CH<sub>3</sub>NH<sub>3</sub>)PbI<sub>3</sub>Sensitized TiO<sub>2</sub> Solar Cells. *J. Phys. Chem. Lett.* **2013**, 4, 2880-2884.
- <sup>20</sup>Zhao, Y.; Nardes, A. M.; Zhu, K. Solid-State Mesostuctured Perovskite CH<sub>3</sub>NH<sub>3</sub>PbI<sub>3</sub> Solar Cells: Charge Trans- port, Recombination, and Di\_ usion Length *J. Phys. Chem. Lett.* **2014**, 5, 490-494.
- <sup>21</sup>Attila J. Mozer, Pawel Wagner, David L. Officer, Gordon G. Wallace, Wayne M. Campbell, Masanori Miyashita, Kenji Sunaharac and Shogo Mori, The origin of open circuit voltage of porphyrin-sensitised TiO<sub>2</sub> solar cells, *Chem. Commun.*, **2008**, 4741–4743.
- <sup>22</sup>Pablo Docampo, Priti Tiwana, Nobuya Sakai, Hidetoshi Miura, Laura Herz, Takurou Murakami, and Henry J. Snaith, Unraveling the Function of an MgO Interlayer in Both Electrolyte and Solid-State SnO<sub>2</sub> Based Dye-Sensitized Solar Cells *J. Phys. Chem. Lett.* **2014**, 5, 490–494.
- <sup>23</sup>Jeong-HyoekIm; Jaehoon Chung; Seung-Joo Kim; Nam-Gyu Park. Synthesis, structure, and photovoltaic property of a nanocrystalline 2H perovskite-type novel sensitizer (CH<sub>3</sub>CH<sub>2</sub>NH<sub>3</sub>)PbI<sub>3</sub>, *Nanoscale Research Letters* **2012**, 7, 353.
- <sup>24</sup>Sigalit Aharon , Bat El Cohen , and Lioz Etgar, Hybrid Lead Halide Iodide and Lead Halide Bromide in Efficient Hole Conductor Free Perovskite Solar Cell, *J. Phys. Chem. C*, **2014**, DOI: 10.1021/jp5023407.

TOC



High voltage hole conductor free perovskite solar cell achieved 1.35V.